Microgravity Sci. Technol. (2016) 28:165–178
DOI 10.1007/s12217-016-9495-8

ORIGINAL ARTICLE

Partial Nucleate Pool Boiling at Low Heat Flux: Preliminary Ground Test for SOBER-SJ10

Ke Wu[1] · Zhen-Dong Li[1] · Jian-Fu Zhao[1] · Hui-Xiong Li[2] · Kai Li[1]

Received: 23 July 2015 / Accepted: 23 February 2016 / Published online: 4 March 2016

Abstract Focusing on partial nucleate pool boiling at low heat flux, SOBER-SJ10, one of 27 experiments of the program SJ-10, has been proposed to study local convection and heat transfer around an isolated growing vapor bubble during nucleate pool boiling on a well characterized flat surface in microgravity. An integrated micro heater has been developed. By using a local pulse overheating method in the experimental mode of single bubble boiling, a bubble nucleus can be excited with accurate spatial and temporal positioning on the top-side of a quartz glass substrate with a thickness of 2 mm and an effective heating area of 4.5 mm in diameter, and then grows under an approximate constant heat input provided by the main heater on the back-side of the substrate. Ten thin film micro-RTDs are used for local temperature measurements on the heating surface underneath the growing bubble. Normal pool boiling experiments can also be carried out with step-by-step increase of heating voltage. A series of ground test of the flight module of SOBER-SJ10 have been conducted. Good agreement of the measured data of single phase natural convection with the common-used empirical correlation warrants reasonable confidence in the data. It is found that the values of the incipience superheat of pool boiling at different subcooling are consistent with each others, verifying that the influence of subcooling on boiling incipience can be neglected. Pool boiling curves are also obtained, which shows great influence of subcooling on heat transfer of partial nucleate pool boiling, particularly in lower heat flux.

Keywords Partial nucleate pool boiling · Boiling incipience · SOBER-SJ10 · Ground test

✉ Jian-Fu Zhao
jfzhao@imech.ac.cn

[1] Key Laboratory of Microgravity/CAS, Institute of Mechanics, Chinese Academy of Sciences, Beijing 100190, China

[2] State Key Laboratory of Multiphase Flow in Power Engineering, Xi'an Jiaotong University, Xi'an 710049, China

Introduction

Boiling heat transfer realizes the high-performance heat exchange due to latent heat transportation both in normal gravity and in microgravity. Boiling process, however, is also a very complex and illusive process because of the interrelation of numerous factors and effects. Such factors and effects, for example, in nucleate pool boiling, include the nucleate process, the growth of the bubbles, the interaction between the heater's surface with liquid and vapor, the evaporation process at the liquid-vapor interface, the transport process of vapor and hot liquid away from the heater's surface, and so on. Furthermore, adding to the complexity is the randomness of the distribution and the configuration of the activated nucleation sites, around which bubbles continue to form, grow up, depart off and move on. Some macro-scale statistical average parameters are then commonly used in the boiling study to fit the needs of engineering endeavors rather than to focus upon the physics of the boiling process. As a result, the literature has been flooded with the correlations involving several adjustable, empirical parameters. These correlations can provide quick input to design, performance, and safety issues and hence are attractive on a short-term basis. However, the usefulness of the correlations diminishes very quickly as parameters of interest start to fall outside the range of physical parameters for which the correlations were developed. Thus, the physics

of the boiling process itself is not properly understood yet, and is poorly represented in the most correlations, despite almost seven decades of boiling research.

So far, several mechanisms of boiling have been proposed, such as evaporation of superheated liquid around a bubble (Han and Griffith 1965a), convective heat transfer induced by bubble rising motion (Forster and Zuber 1955; Haider and Webb 1997), transient heat conduction within a liquid on the surface after bubble departure (Han and Griffith 1965b), microlayer evaporation (Cooper and Lioyd 1969), and more recently, contact line heat transfer (Stephan and Hammer 1994). Some combinations of these mechanisms mentioned above have also been suggested in the literature. Its mechanism, however, has not yet been clarified with common understanding despite of decades of research, and is still the subject of many ongoing research activities all over the world.

It is well known that the most prominent feature of nucleate pool boiling, particularly in partial nucleate pool boiling or isolated bubble regime, is the processes of bubbles' formation, growth and motion around the activated nucleation sites. Thus, the model of single bubble pool boiling has become an attractive model for theoretical study, numerical simulation and experimental observation of nucleate pool boiling phenomenon in order to avoid the influence of the randomness related to the activated nucleation sites and to better reveal the mechanism underlying this phenomenon. Furthermore, the elemental phenomena related to heat transfer in nucleate pool boiling have very small temporal- and spatial-scales. Conventional measurement techniques based on averaged macro-scale parameters can't provide any precise measurement of them and sufficient quantitative verification of the proposed mechanisms. Thanks to advances in technology, many new techniques, such as thermochromic liquid crystals (TLCs), MEMS, high-speed infrared cameras and so on, have been utilized for revealing the physics of nucleate pool boiling.

Kenning and Yan (1996) and Kenning et al. (2001) used thermochromic liquid crystals to study the temperature field at the backside of a 130 μm thick stainless steel plate. They studied the temperature imprint caused by the growth and detachment of a single vapour bubble by focusing on a single nucleation site during fully developed pool boiling. They concluded that constant wall temperature boundary conditions are not applicable in nucleate boiling simulations.

Moghaddam and Kiger (2009) developed a MEMS sensor with 44 platinum thin film resistance temperature detectors radially arranged on a silicon substrate, where thin benzocyclobutene layers with very low thermal conductivity were coated. They measured the continuous bubble boiling of FC-72 under saturation conditions. They pointed out that the transient heat conduction in the liquid thermal boundary layer that formed just after the passage of the advancing contact line is dominant at relatively low wall superheat, and micro-convection heat transfer becomes dominant at high wall superheat because of the shortened bubbling cycle. Contribution of microlayer evaporation and contact line heat transfer was indicated to be small, which was also found by Demiray and Kim (2004) and Myers et al. (2005), who developed a micro heater array sensor with 96 micro heater elements of 100 × 100 μm^2 in size on a quarts or a silica substrate with a heated area 1 mm^2, and conducted a series of boiling experiments of FC-72 under isothermal wall conditions.

Wagner et al. (2007) and Schweizer and Stephan (2009) conducted micro-scale temperature measurements of FC-84, FC3284, and a binary mixture of them by using a high-speed infrared camera, as well as by using thermochromic liquid crystals. They demonstrated that high heat transfer occurred near a three-phase contact line during the advancing and receding processes. They indicated that the contribution of the three-phase contact line heat transfer to the overall wall heat transfer was about 13 %∼30 %.

Using a high-speed infrared camera, Gerardi et al. (2010) showed that the largest enthalpy required for bubble growth is transferred by microlayer evaporation during the saturated boiling of water. Gao et al. (2012) also measured dynamic characteristics of the microlayer beneath an ethanol vapor bubble by using high-speed camera technique and laser interferometric method, while more recently Jung and Kim (2014) measured simultaneously the microlayer shape beneath a de-ionized water vapor bubble by using total internal reflection technique and the temperature distribution on the heating surface by a high-speed, high-resolution infrared thermometry. They reported a wedge-shaped microlayer formed beneath the bubble during the growth period; as the bubble growth it was gradually depleted from the center, creating a dry spot. After the microlayer was completely depleted, the triple-contact line started to recede and the bubble began to depart from the wall.

Yabuki et al. (2012) and Yabuki and Nakabeppu (2014) developed a MEMS sensor with thin film thermocouples and a unique trigger supplying a tiny hydrogen bubble as a bubble nucleus by using the electrolysis of water. They measured the local wall temperature in boiling of water, and found that microlayer evaporation is the dominant mechanism of heat transfer in pool boiling of water. Utaka et al. (2013) used a laser extinction method to measure the microlayer structure in nucleate boiling. They also found that the microlayer is shaped like a wedge, and that during the departure process, the radius of the microlayer decreases, the heat transfer surface becomes covered with bulk liquid again, and the area of the microlayer disappears at some time.

Most recently, Warrier et al. (2015) conducted a series of nucleate pool boiling experiments (NPBX) aboard the International Space Station (ISS). Five cylindrical micro-cavities

were formed on the surface to initiate nucleate boiling. The results of the experiments show that at low superheats, bubbles generated on the heater surface slide and merge to yield a large bubble located in the middle of the heater. At high superheats, the large bubble may lift off from the heater but continue to hover near the surface. In both these scenarios, the large bubble serves as a vapor sink.

Results of studies performed up to date show that a basis for common understanding of nucleate pool boiling phenomena is not yet obtained. More studies, particularly sophisticated experiments on local convection and heat transfer around an isolated growing vapor bubble during partial nucleate pool boiling, are needed. That is the basic motivation of the experiment SOBER-SJ10 (Single bubble pOol Boiling ExpeRiment aboard SJ-10), one of 27 experiments of the program SJ-10 (Hu et al. 2014). The main objective of SOBER-SJ10 is to develop a basic understanding of the local convection, vapor removal, and heat transfer processes around an isolated growing vapor bubble during nucleate pool boiling on a well characterized surface of a flat plate heater in microgravity. It is presently in flight module phase, and the launch of the satellite SJ-10 is scheduled in April, 2016. A detail description of the experimental facility, as well as the measurement methodology, will be provided in the present paper. The results of preliminary ground test of the flight module of SOBER-SJ10 will also be provided and analyzed to reveal the characteristics of partial nucleate pool boiling heat transfer, as well as to verify the function and performance of the developed hardware for future space flight.

Experimental Facility

Based on the scientific objectives of the experiment and the technical constraints of the SJ-10 satellite, the device of SOBER-SJ10 is mainly composed of an air-proof capsule, a boiling chamber, an electric box and two CCD components (Fig. 1). The latter three components are installed inside the air-proof capsule, which is made of aluminium alloy. The pressure inside the air-proof capsule is nominally 100 kPa, while the external pressure of the device is about 50 kPa onboard the SJ-10 satellite. The capsule is sealed by a NBR O-ring in order to obtain a steady pressure condition during the space experiments. The leakage rate is measured as 1.0×10^{-9} Pa·m^3/s. The outer envelope size of the payload is $425 \times 330 \times 280$ mm^3, and the weight is 25 kg.

Boiling Chamber

The schematic of the boiling chamber is shown in Fig. 2. Its major components include one liquid chamber, one cover plate with two end caps, a bellows as a pressure regulator, eight film preheaters, one integrated micro heater, one pre-data acquisition board (pre-DAB) and its support, three LED lighting components, two observation components, and one electric connector.

The total height of the liquid chamber is 234 mm, while its cross section is designed to a regular octagon with a circumcircle diameter of 175 cm in order to facilitate the installation of the major components. Eight film preheaters with the total heating power of 60 W are fixed on the outer walls of the chamber, which are used for adjusting the temperature of the bulk liquid from the ambient temperature to nearly saturation value at the corresponding pressure. Two Pt1000 RTD temperature sensors are fixed on the inner wall and located at the positions corresponding to the centers of two preheaters to measure the inner wall temperature. Their outputs can be used to adjust the pre-heating process to avoid superheating on the inner wall surface of the boiling chamber. The uncertainties are ±1.0 °C in the range from 20 °C to 80 °C according to the results of the pre-calibration.

The integrated micro heater is fixed at the center of the pre-DAB, which is installed at the bottom of the liquid chamber with an inclination angle of 15°. Two Keller® PAA-4LD digital absolute pressure sensors fixed

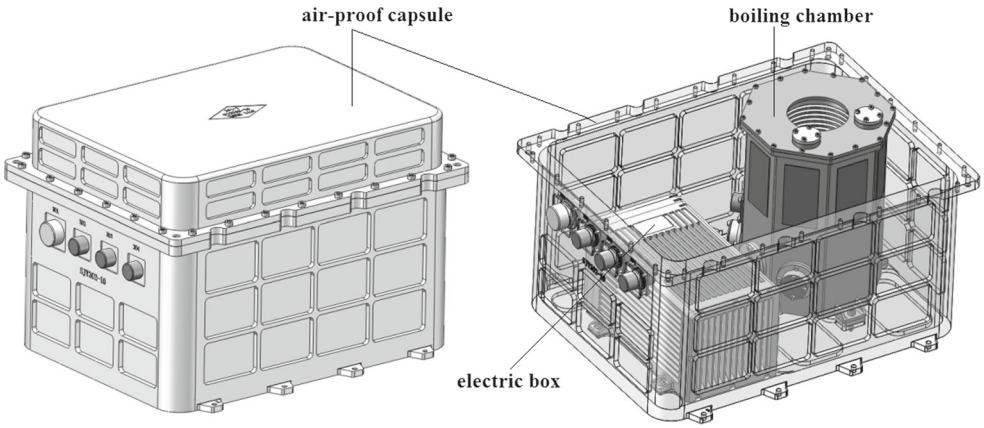

Fig. 1 Schematic of the flight module of SOBER-SJ10

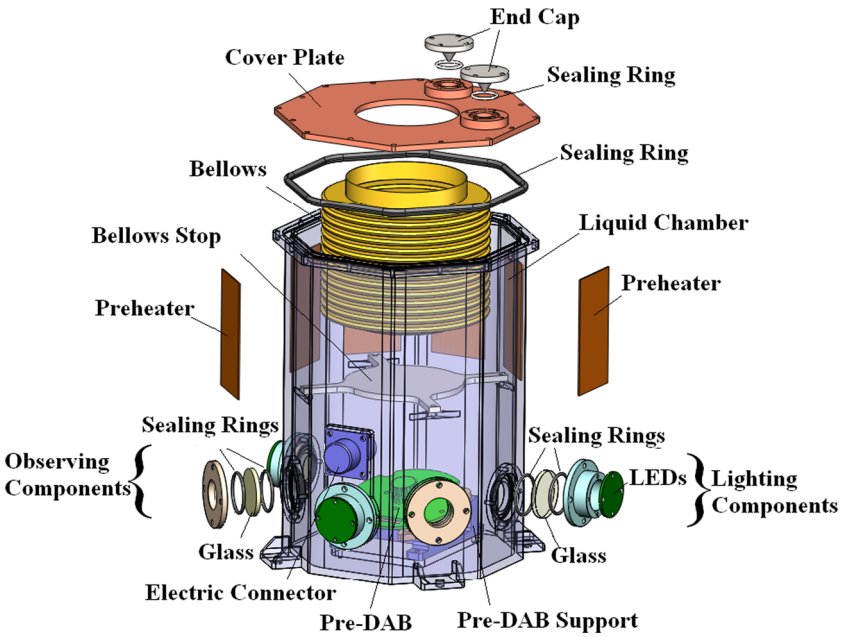

Fig. 2 Schematic of the boiling chamber

on both sides of the integrated micro heater, to measure the pressure inside the boiling chamber and the bulk liquid temperature simultaneously. These sensors locate at the same height as the integrated micro heater, and the distances between centers of the integrated micro heater and each sensor are 33 mm. The ranges of the pressure measurements are 300 kPa, while the uncertainties are ± 1.5 kPa after pre-calibration. For the temperature measurements, the uncertainties are ± 0.2 °C in the range from 20 °C to 80 °C according to the results of the pre-calibration.

Three LED lighting components and two observation components are set alternately in front of the heater. Thus, the front and the side lighting can provide adequate illumination, while two observation windows can provide orthogonal images of the growth and motion of vapor bubble near the integrated micro heater.

A beryllium bronze bellows, which is connected with the cover plate of the liquid chamber, acts as a pressure regulator to maintain the pressure inside the chamber approximately constant during the preheating and boiling processes with the help of constant background pressure environment inside the air-proof capsule. In order to prevent the excessive elongation of the bellows, a bellows stop is set at the middle of the chamber. After deducting the volume of the bellows and other parts inside the chamber, the effective volume of the liquid chamber is about 2.8 L.

Integrated Micro Heater

The integrated micro heater is fabricated by using MEMS technique. The substrate of the integrated micro heater is a $10 \times 10 \times 2$ mm^3 quartz glass wafer. The thickness of 2 mm was determined by a prior numerical study (Zhang et al. 2015; Li et al. 2015). Figure 3 shows the configurations of the electro-circuits on the top- and back-sides of the substrate, which was fabricated by using the standard photolithography technique for the patterning of the sensor design and magnetron sputtering for film deposition. Here, the top-side refers to the heating surface contacting directly with the working fluid.

At the center of the top-side, there is a pulse bubble trigger for exciting a bubble nucleus by using the method of local overheating. Around the bubble trigger, there are two groups of thin film micro-RTDs for local temperature measurements on the heater surface which are distributed uniformly in the circumferential direction (Fig. 3b). Each group has 5 series local temperature sensors. The distances of these local temperature sensors from the center of the bubble trigger, shown in Fig. 3c, are listed in Table 1. The bubble trigger, the sensors and the lead wires are all formed by thin platinum films of about 300 Å in thickness. For the sake of safety, the bubble trigger is composed of two parallel platinum films with a size of 100×20 µm^2 and a spacing of 20 µm (Fig. 3c). Each local temperature sensor with a nominal electric resistance of 1 kΩ is composed of a serpentine strip of platinum film covering on an area of 55×50 µm^2. About 4000 Å-thick gold layers are covered on all pads for bridge-connecting with external circuit. Furthermore, a 200 Å-thick SiO_2 layer is covered on the top-side of the substrate to protect the trigger and the local temperature sensors, as well as to smooth the heating surface.

On the back-side of the substrate, a serpentine strip of platinum film of about 5000 Å in thickness acts simultaneously as the main heater to provide the input power for maintaining the boiling process and the temperature sensor to measure the average temperature on the back-side of the

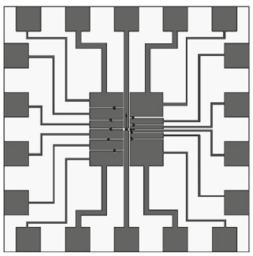

a) top-view of the substrate

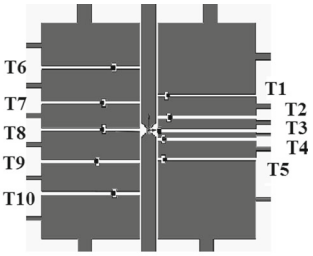

b) enlarged view of the center area of the heating surface on the top-side

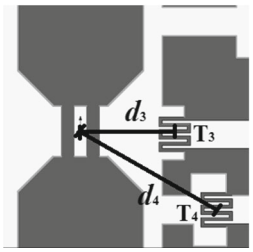

c) enlarged view near the bubble trigger on the top-side

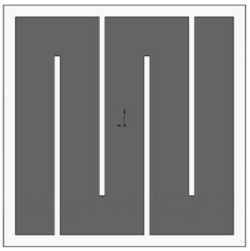

d) bottom-view of the substrate

Fig. 3 Configurations on the top- and back-sides of the substrate of the integrated micro heater

substrate (Fig. 3d). The nominal electric resistance of the main heater is 4 Ω.

A kind of plastic package, COB (chip on board) encapsulation, is used to encapsulate the integrated micro heater as an independent electronic component (Fig. 4). Two PCBs of 1.6 mm in thickness are used to provide electric connections and mechanical support for the integrated micro heater. The main heater is welded on the lower PCB by using the surface mount method, while the bubble trigger and local temperature sensors are bridge-connected with the upper PCB by double gold wires with a diameter of 25 μm. 2 pins are connected with each end of the main heater on the back-side of the substrate for a good reliability, while only one pin is connected with each pad on the top-side. Each pin has a 0.5×0.5 mm^2 square cross-section and a length of about 20 mm. Finally, the substrate, as well as all gold wires, is packaged on the PCBs by using the packaging adhesive DOVER DE108.

An effective heating area with a diameter of 4.5 mm can contact the liquid directly. It is slightly lower than the chip surface. Thus, an inclination angle of 15° with the horizontal bottom of the boiling chamber is adopted for the pre-DAB in order for clear observations of the shape and the motion of the growing bubble on the top surface of the integrated micro heater. The center line is along the bubble trigger and its leads. And then the sensor T6, located at the position of 11 o'clock, is the highest one relative to the bottom of the boiling chamber among all local temperature sensors.

Working Fluid

Degassed FC-72 with a nominal volume of about 2.8 L was used as the working fluid. FC-72 is an isomeric mixture of perfluorohexane. The principle component is n-perfluorohexane, an isomer with a linear arrangement of the carbon atoms. The carbon atoms in the other isomers of C_6F_{14} are branched.

The air concentration in the liquid was reduced by repeatedly pulling a vacuum on the vapor/air above the liquid in the boiling chamber, while the liquid temperature was kept at a higher value of about 50 °C. The pressure above the liquid was lowered long enough to boil the liquid repeatedly, ensuring that all of the vapor/air was removed. Once the liquid was degassed, the pressure around the bellows was brought up to 1 atm. Since there was almost no pressure difference across the seals in the boiling chamber,

Table 1 The distances d_i of local temperature sensors from the center of the trigger

Sensors	T1	T2	T3	T4	T5	T6	T7	T8	T9	T10
d_i (mm)	0.55	0.35	0.15	0.25	0.45	1.0	0.75	0.65	0.85	1.0

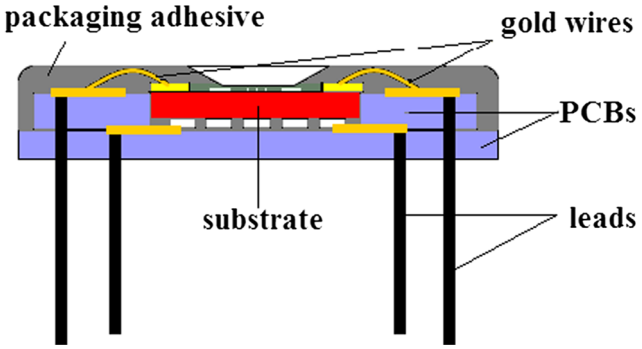

Fig. 4 Schematic of the integrated micro heater with a COB package (not to scale)

gas infiltration back into the liquid through the seals was minimized.

For a given partial pressure of gas (p_g) above the liquid, the dissolved gas concentration c_g (moles gas/mole liquid) in the liquid phase is given by Henry's law

$$c_g = H\,(T)\,p_g \tag{1}$$

where $H(T)$ is Henry's constant at liquid temperature T. For air in FC-72, H has been measured to be 5.4×10^{-8} mole/(mole·Pa) at the range from 31 °C to 60 °C (Henry et al. 2006). It may slightly decrease with the decreasing temperature (You et al. 1995). The air partial pressure p_g can be determined from a measurement of the total pressure p_T of the gas above the liquid and the bulk liquid temperature (t_{bulk}) after the two-phase system has come to equilibrium in a sealed container, i.e.

$$p_g = p_T - p_{sat}\,(t_{bulk}) \tag{2}$$

where $p_{sat}(t_{bulk})$ is the saturation pressure of the liquid at the measured temperature t_{bulk} and can be determined from

$$p_{sat}\,(t) = 10^{9.729-1562/(t+273.15)} \tag{3}$$

It ought to be pointed out that the uncertainties of the sensors for measuring the pressure and temperature are estimated to induce an uncertainty of about 70 ppm for the gas concentration. Furthermore, the uncertainty of the saturation pressure formula, e.g. Eq. 3, may also induce some considerable uncertainty for the gas concentration.

Presently, a small amount of fresh FC-72 was added into the carefully degassed FC-72 inside the boiling chamber after the first ground test GE1, in order to maintain a suitable initial end position of the bellows. It will cause a slight increase of the final air concentration in the bulk liquid in the boiling chamber. Further degassing operation will be done before the space flight to reduce the final air concentration.

During the thermal test of the facility SOBER-SJ10 on the ground, the pressure in the boiling chamber reaches its saturated value at about 1 °C and then jumps abruptly with

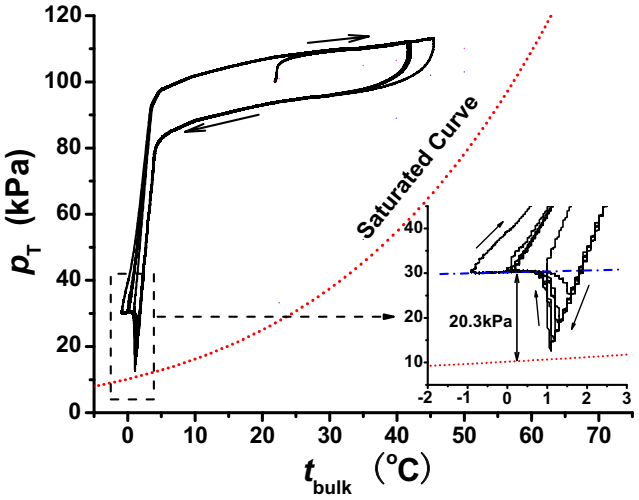

Fig. 5 Change of bulk liquid state during the ground thermal test of SOBER-SJ10

the further decrease of bulk liquid temperature (Fig. 5). The pressure shows a very slight decrease with further decrease of temperature until the temperature rises again. It indicates that the vapor/air phase exists above the liquid in the boiling chamber, which is caused by the fixed volume after the bellows stop is activated. By correcting the effect of the static pressure, the air partial pressure p_g above the liquid can be determined as 20.3 kPa, and the final dissolved gas concentration c_g in the liquid phase is about 1100 ppm if the value of 5.4×10^{-8} mole/(mole·Pa) is assumed.

Data Acquisition and Video Record

Throughout the whole process of space flight experiment, including boiling stages and others, all important parameters, such as the bulk liquid temperature, the inner wall temperature of the liquid chamber, the pressure inside the bulk liquid, the voltage across the main heater and those across 10 local temperature sensors and 3 reference resistances for the corresponding current measurements, are sampled at a low sampling frequency of 1/3 Hz. These low frequency sampling data are transmitted to the payload manager in the pressurized module of the satellite SJ-10 through a RS485 interface.

A high sampling frequency of 500 Hz are used during boiling stages for the integrated micro heater signals, namely the voltage across the main heater and those across 10 local temperature sensors and 3 reference resistances for the corresponding current measurements in order to obtain adequate time resolution. These high frequency sampling data are transmitted firstly to a FPGA unit through a RS422 interface, packaged with 2 series of compressed video data, and then transmitted to the payload manager through a LVDS interface.

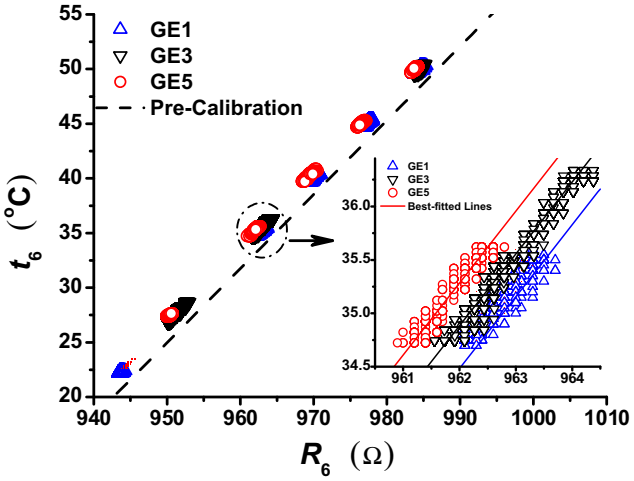

Fig. 6 Typical results of the syn-calibrations of the local temperature sensor T6

Two Watec® WAT-660D CCDs with a resolution of 537(H) × 505(V) pixels are installed in two orthogonal directions to obtain videos of the shape and the motion of the growing bubble, which can be used to reconstruct the true shape of the growing bubble. Furthermore, these images can also act as a redundancy backup of each other to improve reliability. The analog video signals of the two CCD cameras are converted firstly into BT656 digital video signals, and then encoded by using H.264 video compression format. The two compressed video signals, as well as the high frequency sampling data mentioned above, are packaged by the FPGA unit and then transmitted to the payload manager through a LVDS interface.

Since the facility SOBER-SJ10 can't be recovered after space flight, all the data will be transmitted back to the ground through the remote transmission system when the satellite SJ-10 flies over the mainland of China. Furthermore, all data reported in the present paper are also obtained from the same system as that used in the future space flight experiment, except the remote transmission system.

Experimental Procedure and Data Reduction

The planned space experiment will be executed automatically for about 15 hours, which is divided into 5 stages. The first stage is carried out at ambient temperature in a range from 0 to 30 °C without pre-heating process, while the others are carried out at higher temperatures of 35 °C, 40 °C, 45 °C, and 50 °C, respectively. The pre-heaters will be switched on when the bulk liquid temperature is 0.2 °C less than the designed value of the bulk liquid temperature at each stage, and switched off when the designed value is reached. Furthermore, the pre-heaters will also be switched off if the inner wall temperature is larger than 60 °C to avoid boiling on the inner wall surface of the chamber. It is verified on the ground that the adjusted range of the bulk liquid temperature is no more than ±1.0 °C around the set value.

In each stage, there are 5 individual runs. The first 4 runs are designed as the single bubble boiling mode, in which a bubble nucleus will be excited by the activated pulse bubble trigger and then grow under the action of the main heater on the back-side of the substrate of the integrated micro heater. The heating voltage upon the main heater is kept constant in each run and increases in the successive runs. The last run of each stage is designed as the normal pool boiling mode, in which the bubble trigger is not activated, while the heating voltage of the main heater, by contrast with those in the single bubble boiling mode, will be adjusted increasing step by step. Abbreviations, such as GE1/2.4, which refers to the fourth run of the second stage in the first ground test, are

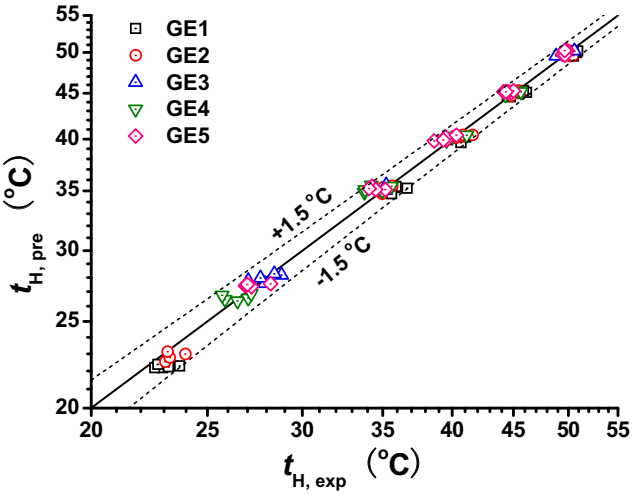

Fig. 7 Syn-calibration for the main heater of the integrated micro heater

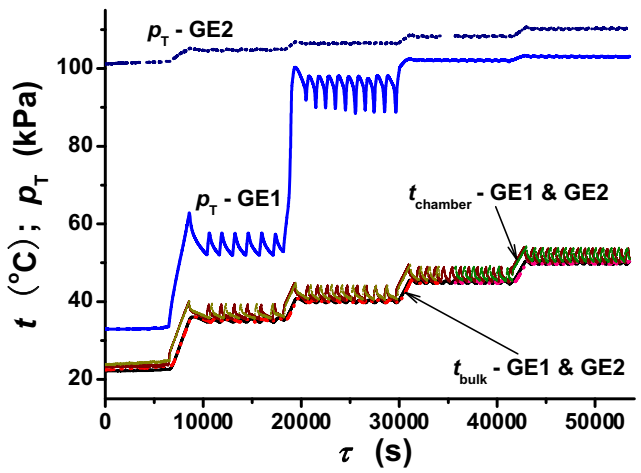

Fig. 8 Typical change of bulk liquid state with time during the first two ground tests

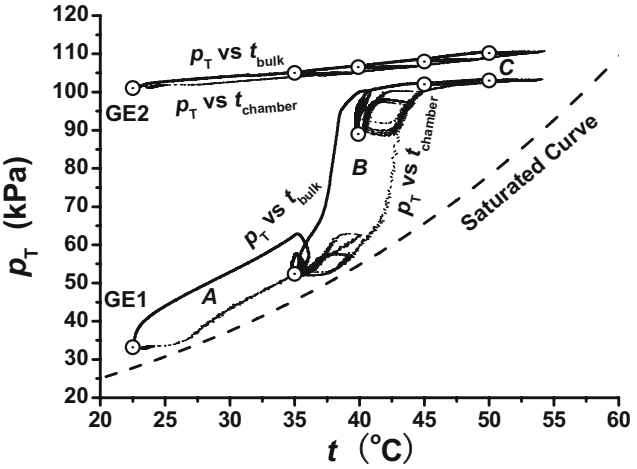

Fig. 9 Typical change of bulk liquid state comparing with the saturated curve of FC-72 during the first two ground tests

used to denote the condition of each experimental run in the following sections.

As mentioned above, both the main heater and local temperature sensors, particularly the latter, are made of thin platinum films, which may exhibit obvious effects of zero shifts. A syn-calibration procedure for local temperature sensors is carried out to avoid the effects of zero shifts on the calculated values of the measured temperatures. In the syn-calibrations, in order to avoid the influence of transient electric heating effect both from the main heater of the integrated micro heater inside the working fluid and from the pre-heaters outside the boiling chamber, the data obtained during pre-heating processes when the liquid temperature does not reach the predetermined values, as well as those during every individual run when the main heater is switched on, will be removed at first. Furthermore, transient data after each individual run will also be removed, to eliminate any effects of heat input both from the main heater of the integrated micro heater inside the working fluid and from the pre-heaters outside the boiling chamber. Then, by using the measured corresponding resistances and the bulk liquid temperature at the designed states of bulk liquid, the temperature-resistance correlations of the local temperature sensors can be calibrated and used to calculate the local temperature during every individual run in the same test.

Figure 6 shows, for example, the syn-calibrations for local temperature sensor T6 in the first, the third, and the fifth ground tests. For the sake of clarity, the data in GE2 and GE4 aren't shown in Fig. 6. The average bulk liquid temperature based on the outputs of temperature from two Keller® PAA-4LD digital absolute pressure sensors is used as the reference temperature. It is shown in Fig. 6 that there exists an obvious effect of zero shifts. Although a linear relationship can be obtained and the slope was kept constant in different tests, the intercept of the temperature-resistance correlation is generally found to change little with the aged surface. The same phenomenon was also observed by Merte et al. (1998) for thin gold film heater.

By using the syn-calibration procedure mentioned above, the uncertainties of local temperature sensors are confirmed to be less than ±1.0 °C. Furthermore, caused by the uncertainty of the pressure measurement, an uncertainty of about ±0.5 °C may arise for the saturate temperature of FC-72. Thus, the uncertainty of the wall superheat will be no more than ±1.5 °C.

The same procedure of the syn-calibration was also used for the resistance-temperature relationship of the main heater. The result is shown in Fig. 7. Contrary to local temperature sensors, no obvious zero shift occurs here, which may be caused by the relatively thicker film thickness of the main heater comparing with those of local temperature sensors. Thus, the result of the pre-calibration can be used to determine the temperature on the back-side of the substrate of the integrated micro heater, while the syn-calibration to verify its validity. It is confirmed in Fig. 7 that the uncertainty of the temperature on the back-side of the substrate is less than ±1.5 °C.

As mentioned above, a 200 Å-thick SiO_2 layer is covered on the top-side of the substrate of the integrated micro heater to protect the trigger and the local temperature sensors, as well as to smooth the heating surface. Thus, the heater surface contacting directly with the working fluid can be well considered as an isotropic one with the same surface roughness and contact angle everywhere. Therefore, the shape of the growing bubble, as well as the distribution of temperature underneath the bubble, will be axisymmetric both in the horizontal case in normal gravity and in microgravity. The measurements of local temperature at discrete

Table 2 Conditions of each stage in the fifth ground test GE5

Stage	Bulk liquid temperature (°C)	Liquid pressure (kPa)	Saturated temperature (°C)	Subcooling (°C)
GE5/1	27.5	101.6	57.8	30.2
GE5/2	35.2	102.6	58.0	22.8
GE5/3	40.0	103.3	58.3	18.2
GE5/4	45.2	104.6	58.7	13.5
GE5/5	50.0	111.3	60.4	10.4

points can represent the values at the same distances from the bubble trigger. By using the interpolation technique, the spatiotemporal distribution of local temperature on the heating surface can then be obtained based on the data obtained from these ten local temperature sensors, which also provides a proper boundary condition on the top-side of the substrate. A uniform boundary condition on the bottom-side can be determined based on the data obtained from the main heater, too. Furthermore, an adiabatic condition can be reasonably assumed on the outer boundary at certain radius. Thus, once the temperature distributions on the top-side and on the back-side of the substrate are obtained, the transient heat conduction calculation inside the substrate during the boiling process may be straightforward by using a proper algorithm for the axisymmetric two dimensional heat conduction. This procedure can be applied to the single bubble boiling mode, particularly in microgravity.

Furthermore, for normal pool boiling and for natural convection from the top surface of the integrated micro heater, the temperature distribution on the top surface is fairly uniform and steady in the terminal period after the constant heating voltage is acted upon the main heater. Thus, the heat flux from the heater to the working fluid can be calculated directly as follows

$$q = \lambda \left(t_{bottom} - t_{top}\right)/h \tag{4}$$

here, λ and h denote the thermal diffusivity and the thickness of the substrate of the integrated micro heater, respectively. The uncertainty of the heat flux from the heater to the working fluid is estimated not to be more than ±6 % of the calculated value.

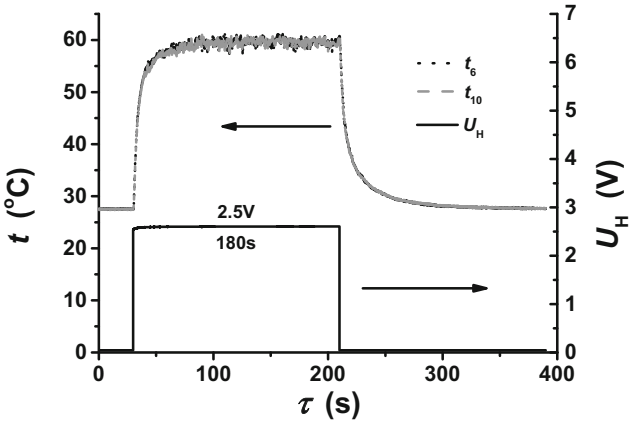

Fig. 10 Historigrams of the heating voltage and the corresponding local temperatures on the top surface during a single bubble boiling run (GE5/1.4)

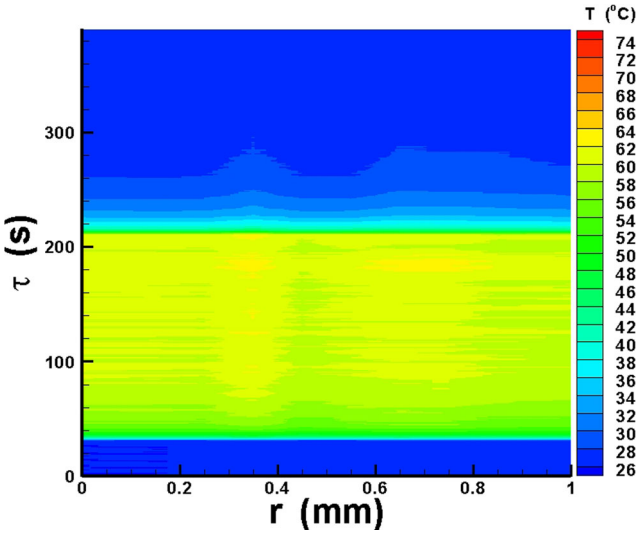

Fig. 11 Spatiotemporal distribution of local temperature on the heating surface of the integrated micro heater during a single bubble boiling run (GE5/1.4)

Heat Transfer of Partial Nucleate Pool Boiling in Normal Gravity

During the development of the facility SOBER-SJ10, particularly in the flight module phase, a series of ground tests have been conducted to verify its functional features and performances, as well as to obtain experimental data in normal gravity for comparing with those obtained in the future space flight experiments. The typical changes of bulk liquid state during the first two ground tests are shown in Figs. 8 and 9. The designed states for five stages are shown as discrete points in Fig. 9.

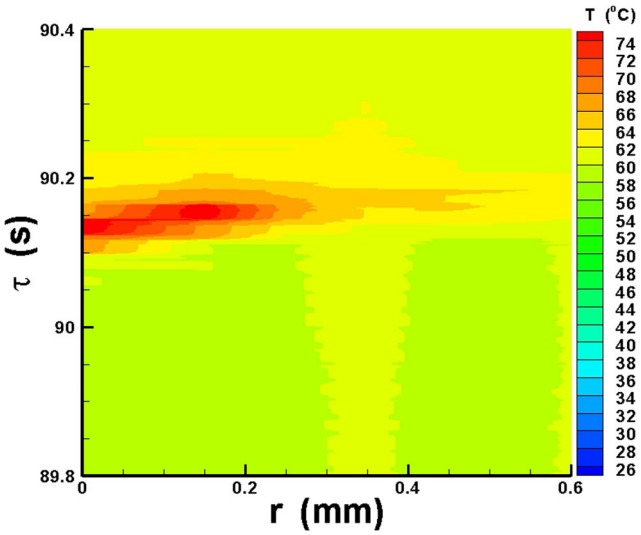

Fig. 12 Enlarged view of Fig. 11 near the activation of pulse bubble trigger

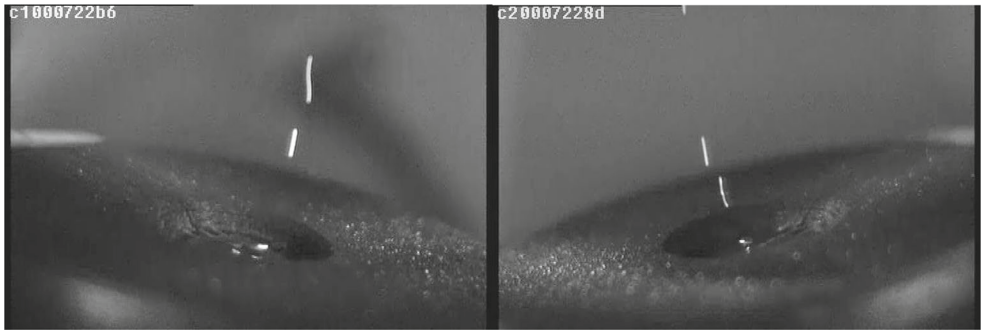

Fig. 13 CCD images of bubble movement in a single bubble boiling run (GE5/1.4)

In the first ground test GE1, a dramatic change of the pressure occurs near the bulk temperature of 40 °C, which is caused by insufficient quantity of filled working fluid. Generally, the working fluid will expand when heated and contract when cooled. Thus, the bellows stop will activate and then the effective volume of the boiling chamber is fixed when the temperature of bulk liquid is smaller than some value. Further decrease of the temperature of bulk liquid will result in evaporation and appearance of liquid-vapor interface. It is also shown that, in the two low temperature stages of the test GE1, there is a nearly constant difference of 5.4 kPa between the measured total pressure and the saturate pressure of FC-72 at the corresponding bulk liquid temperature. As discussed above, this difference is equal to the air partial pressure above the liquid. The dissolved gas concentration of 200 ppm in the liquid phase is then given by Henry's law with the correction of the effect of the static pressure, which is much smaller than 1100 ppm in the successive ground tests as mentioned above. The reason for this difference is that more thorough degassing process was done before GE1, while a small amount of fresh FC-72 was added into the boiling chamber to maintain a suitable initial end position of the bellows for the sake of safety after GE1. Due to the requirements of the SJ-10 project schedule, further degassing is planned to be done just prior to the space flight.

After readjusting the quantity of the filling liquid, the change of the pressure in the boiling chamber is smaller throughout the second ground test GE2. In other successive ground tests, the changes of the pressure in the boiling chamber are the same as that in GE2 and then not shown in Figs. 8 and 9 for the sake of clarity. The dissolved gas concentration in the liquid phase, as mentioned above, is 1100 ppm. It ought to be noted here that, according to You et al. (1995) and Rainey et al. (2003), dissolved gas was found to influence boiling incipience only at high gas concentrations (>5000 ppm). Furthermore, it is thought that the presence of dissolved gas does not have a dramatic influence on the ebullition cycle. Therefore, the data reported here with the dissolved gas concentration of 1100 ppm may be useful to reveal heat transfer of partial nucleate pool boiling of FC-72 in normal gravity, though it is believed that the

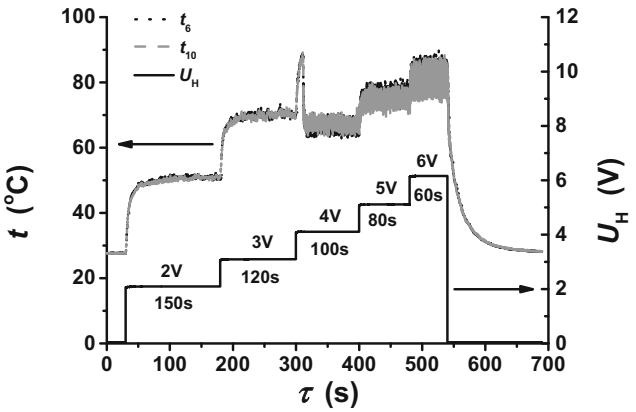

Fig. 14 Historigrams of the heating voltage and the corresponding local temperatures on the top surface during a normal pool boiling run (GE5/1.5)

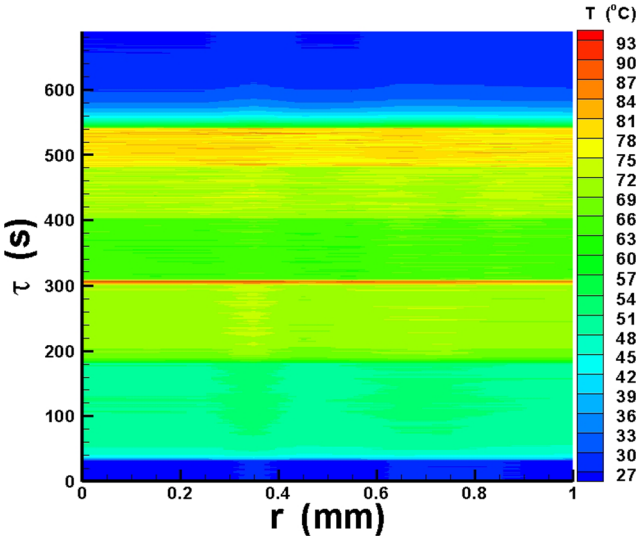

Fig. 15 Spatiotemporal distribution of local temperature on the heating surface of the integrated micro heater during a normal pool boiling run (GE5/1.5)

dissolved gas in the liquid phase may exhibit a more important effect on pool boiling in microgravity.

Table 2 lists the conditions of each stage in the fifth ground test GE5, which will be discussed in detail here. In this ground test, the heating surface was adjusted to the horizontal upward direction.

Figure 10 shows a typical historigram of local temperature on the heating surface of the integrated micro heater and the heating voltage acted upon the main heater during a ground experimental run of single bubble boiling (GE5/1.4). For the sake of clarity, only two outputs from the local temperature sensors T6 and T10, both located at $r = 1.0$ mm, are shown in the figure. The consistency between these two data shows, in a sense, that the effects of the inclination of the heating surface, if existed, can be neglected.

No persistent boiling occurs in the run of single bubble boiling mode (GE5/1.4), which is caused both by the strong natural convection in normal gravity and by the high subcooling (~30 °C). Only in two runs of single bubble boiling mode, namely GE5/4.4 and GE5/5.4, at lower subcooling with the highest heating voltage (2.5 V), persistent boiling occurred after the pulse bubble trigger was activated.

Assuming an axisymmetric distribution of local temperature underneath the growing bubble, the spatiotemporal distribution of local temperature on the heating surface can then be obtained by using the interpolation technique based on the data from these ten local temperature sensors. Figure 11 shows the spatiotemporal distribution of local temperature on the top surface of the integrated micro heater in GE5/1.4. As shown in Fig. 10, the main heater is switched on at 30 s, and then switched off at 210 s in this run. A relative uniform distribution of temperature along the radial direction is evident in Fig. 11. Small ripples may be caused mainly by the random noise both of the physical process and of the measurement.

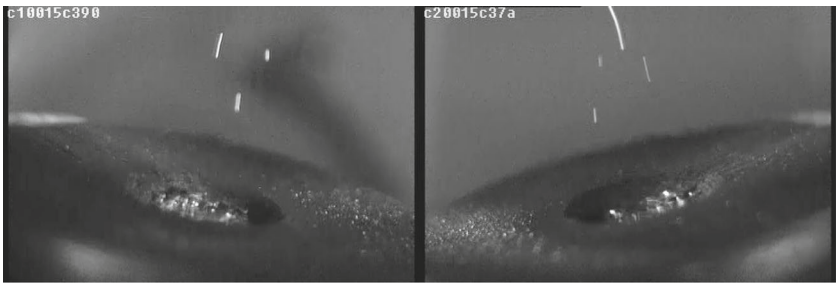

a) heating voltage: 4V

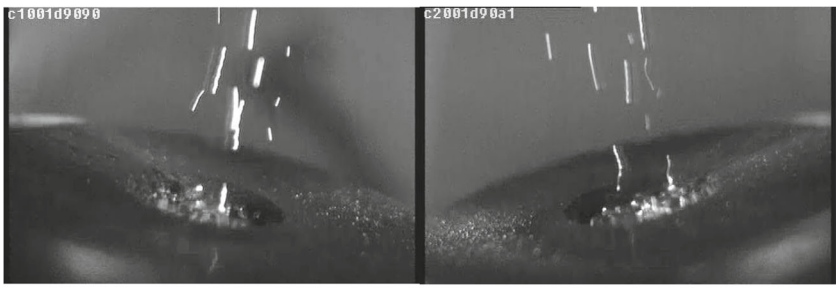

b) heating voltage: 5V

c) heating voltage: 6V

Fig. 16 CCD images of bubble movement in the normal boiling run (GE5/1.5)

An enlarged view of Fig. 11 near the activation of bubble trigger is shown in Fig. 12. The pulse bubble trigger was activated at about 90 s and lasted 50 ms. A local superheated area can be observed clearly. Video playback shows that, in addition to the activation of bubble trigger when there are only several bubbles observed departing quickly from the center of the heating surface (Fig. 13), no bubble can be observed.

Figure 14 show a typical historigram of local temperature on the heating surface of the integrated micro heater and the heating voltage acted upon the main heater during a ground experimental run of normal pool boiling (GE5/1.5). It can be observed clearly that the incipience of nucleate pool boiling occurs with a dramatic drop of the temperature at the beginning of the third step of heating voltage. The averaged temperature of the heating surface increases with the increasing heating power both in the regime of single phase natural convection and in the regime of nucleate pool boiling. This trend can not be maintained in different regimes. Furthermore, the temperature fluctuations become more intense after the boiling incipience, while the increase of the averaged temperature of the heating surface decreases comparing with that in the regime of single phase natural convection.

Figure 15 shows spatiotemporal distribution of local temperature on the heating surface of the integrated micro heater in GE5/1.5. A relative uniform and steady distribution of temperature along the radial direction is also evident during each step of heating voltage, which means the heating time for every step is appropriate to obtain steady state of nucleate pool boiling, at least in normal gravity.

Figure 16 shows some typical bubble behaviors in the latter three steps of heating voltage in GE5/1.5. With increasing heating voltage, more bubbles are excited, and the bubble detach frequency increase, too.

Figure 17 shows the heat transfer curve based on the temperature difference between the wall and the bulk liquid in normal gravity. Data except unsteady ones are calculated in the final steady windows of each heating voltage by using Eq. 4, in which the temperature of the top-side is obtained by averaging all data from the ten local temperature sensors. The unsteady data, marked with a larger circle in Fig. 17, are calculated also by Eq. 4 just before the boiling incipience, which may not reach equilibrium, and thus may overestimate the heat flux. In the regime of single phase natural convection, the heat transfer curves, both in different subcooling conditions and in different test modes, can merge with each other, and be also consistent with the prediction by the common-used empirical correlation (Holman 2005). More obvious effects of the subcooling on the heat transfer curves are observed in the partial nucleate pool boiling regime. Two points of persistent boiling occurred after the pulse bubble trigger was activated in the runs of single bubble boiling mode, namely GE5/4.4 and GE5/5.4, show the same trend as that in the runs of normal boiling mode. It is, however, shown that there is a slight deterioration of heat transfer compared with that in the normal boiling mode. It is mainly caused by the fact that nucleation is only excited at the bubble trigger in these cases, and thus the effective area of boiling surface becomes smaller than that in the normal boiling mode where nucleation sites are distributed on the whole heating surface.

Figure 18 shows the conventional boiling curves at different subcooling in GE5. For sake of clarity, only the data obtained from the runs of normal pool boiling are shown in this figure. Data of Kim et al. (2002) with similar dissolved gas concentration (<1500 ppm) and a smaller heating area

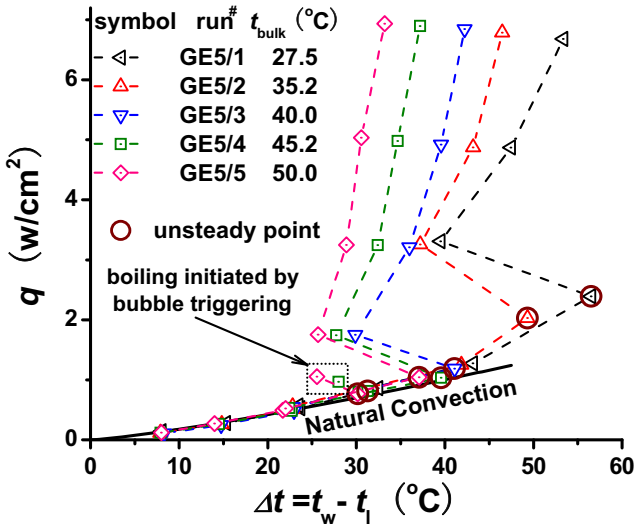

Fig. 17 Heat transfer curve based on the temperature difference between the wall and the bulk liquid in normal gravity

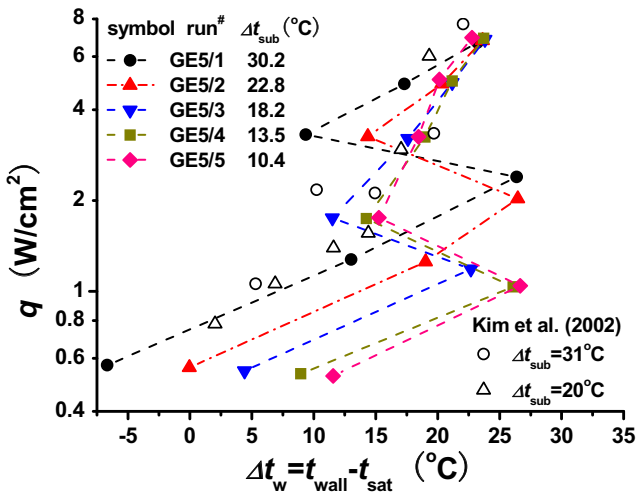

Fig. 18 Pool boiling curve at different subcooling conditions in normal gravity

(2.7×2.7 mm^2) are also shown for comparison. In general, the present data are in good satisfaction comparing with those of Kim et al. (2002). A relatively larger overshoot of wall superheat occurs apparently in the present experiment, which are in unsteady state as mentioned above. The values, however, of the unsteady incipience superheat of pool boiling at different subcooling are consistent with each others, verifying that the influence of subcooling on boiling incipience can be neglected (Straub 2001). The greater the subcooling is, the higher the heat transfer efficiency of partial nucleate pool boiling at low heat flux. The difference, however, decreases quickly with the increase of heat flux, which can be completely disappeared at the maximum heat flux adopted in the present study.

Conclusions

Focusing on partial nucleate pool boiling at low heat flux, SOBER-SJ10, one of 27 experiments of the program SJ-10, has been proposed to study local convection and heat transfer around an isolated growing vapor bubble during nucleate pool boiling on a well characterized flat surface in microgravity. It is presently in flight module phase, and the launch of the satellite SJ-10 is scheduled in April, 2016. The hardware of the flight module of SOBER-SJ10, as well as the experimental procedure and data reduction method, is detailed in the present paper.

A series of ground tests of the flight module of SOBER-SJ10 have been conducted to reveal the characteristics of partial nucleate pool boiling heat transfer, as well as to verify the function and performance of the developed hardware for future space flight. It is found in the ground tests that,

(1) The heat transfer curves at different subcooling conditions can merge together in the single phase natural convection regime and agree well with the prediction by the common-used empirical correlation, which warrants reasonable confidence in the data.
(2) The values of the incipience superheat of pool boiling at different subcooling are consistent with each others, verifying that the influence of subcooling on boiling incipience can be neglected.
(3) The greater the subcooling is, the higher the heat transfer efficiency of partial nucleate pool boiling at low heat flux. The difference, however, decreases quickly with the increase of heat flux, which can be completely disappeared at the maximum heat flux adopted in the present study.

Furthermore, the results of the preliminary ground tests of the flight module of SOBER-SJ10 show that it works well as expected, and then can meet the requirements of the future space experiments to obtain good data on pool boiling heat transfer in microgravity both in the single bubble boiling mode and in the normal pool boiling mode.

Acknowledgements The present study is supported financially by the Strategic Priority Research Program on Space Science, the Chinese Academy of Sciences under the grant of XDA04020404, and the National Natural Science Foundation of China under the grants of 11372327 and 11402273.

References

Cooper, M.G., Lioyd, A.J.P.: The microlayer in nucleate pool boiling. Int. J. Heat Mass Transf. **12**, 895–913 (1969)
Demiray, F., Kim, J.: Microscale heat transfer measurements during pool boiling of FC-72: effect of subcooling. Int. J. Heat Mass Transf. **47**, 3257–3268 (2004)
Forster, H.K., Zuber, N.: Dynamics of vapor bubbles and boiling heat transfer. AICHE J. **1**, 531–535 (1955)
Gao, M., Zhang, L.X., Cheng, P., Quan, X.J.: An investigation of microlayer beneath nucleation bubble by laser interferometric method. Int. J. Heat Mass Transf. **57**, 183–189 (2012)
Gerardi, C., Buongiorno, J., Hu, L., McKrell, T.: Study of bubble growth in water pool boiling through synchronized, infrared thermometry and high-speed video. Int. J. Heat Mass Transf. **53**, 4185–4192 (2010)
Haider, S.I., Webb, R.L.: A transient micro-convection model of nucleate pool boiling. Int. J. Heat Mass Transf. **40**, 3675–3688 (1997)
Han, C.Y., Griffith, P.: The mechanism of heat transfer in nucleate pool boiling, part I, bubble initiation, growth and departure. Int. J. Heat Mass Transf. **8**, 887–904 (1965a)
Han, C.Y., Griffith, P.: The mechanism of heat transfer in nucleate pool boiling, part II, the heat flux-temperature difference relation. Int. J. Heat Mass Transf. **8**, 905–914 (1965b)
Henry, C.D., Kim, J., McQuillen, J.: Dissolved gas effects on thermocapillary convection during boiling in reduced gravity environments. Heat Mass Transf. **42**, 919–928 (2006)
Holman, J.P.: Heat Transfer, 9th edn. McGraw-Hill Education (Asia) Co./China Machine Press (2005)
Hu, W.R., Zhao, J.F., Long, M., et al.: Space program SJ-10 of microgravity research. Microgravity Sci. Technol. **26**, 159–169 (2014)
Jung, S., Kim, H.: An experimental method to simultaneously measure the dynamics and heat transfer associated with a single bubble during nucleate boiling on a horizontal surface. Int. J. Heat Mass Transf. **73**, 365–375 (2014)
Kenning, D.B.R., Yan, Y.: Pool boiling heat transfer on a thin plate: features revealed by liquid crystal thermography. Int. J. Heat Mass Transf. **39**, 3117–3137 (1996)
Kenning, D.B.R., Kono, T., Wienecke, M.: Investigation of boiling heat transfer by liquid crystal thermography. Exp. Thermal Fluid Sci. **25**, 219–229 (2001)
Kim, J., Benton, J.F., Wisniewski, D.: Pool boiling heat transfer on small heaters: effect of gravity and subcooling. Int. J. Heat Mass Transf. **45**(19), 3919–3932 (2002)
Li, Z.D., Zhang, L., Zhao, J.F., Li, H.X., Li, K., Wu, K.: Numerical simulation of bubble dynamics and heat transfer with transient thermal response of solid wall during pool boiling of FC-72. Int. J. Heat Mass Transf. **84**, 409–418 (2015)
Merte, H., Lee, H.S., Keller, R.B.: Dryout and rewetting in the pool boiling experiment flown on STS-72 (PBE-II B) and STS-77 (PBE-II A). NASA/CR-1998-207410, Lewis Research Center, USA (1998)

Moghaddam, S., Kiger, K.: Physical mechanisms of heat transfer during single bubble nucleate boiling of FC-72 under saturation conditions—I. experimental investigation. Int. J. Heat Mass Transf. **52**, 1284–1294 (2009)

Myers, J.G., Yerramilli, V.K., Hussey, S.W., Yee, G.F., Kim, J.: Time and space resolved wall temperature and heat flux measurements during nucleate boiling with constant heat flux boundary conditions. Int. J. Heat Mass Transf. **48**, 2429–2442 (2005)

Rainey, K.N., You, S.M., Lee, S.: Effect of pressure, subcooling, and dissolved gas on pool boiling heat transfer from microporous surfaces in FC-72. ASME J. Heat Transf. **125**(1), 75–83 (2003)

Schweizer, N., Stephan, P.: Experimental study of bubble behavior and local heat flux in pool boiling under variable gravitational conditions. Multiphase Sci. Technol. **21**, 329–350 (2009)

Stephan, P., Hammer, J.: A new model for nucleate boiling heat transfer. Heat Mass Transf. **30**, 119–125 (1994)

Straub, J.: Boiling heat transfer and bubble dynamics in microgravity. Adv. Heat Transf. **35**, 57–172 (2001)

Utaka, Y., Kashiwabara, Y., Ozaki, M.: Microlayer structure in nucleate boiling of water and ethanol at atmospheric pressure. Int. J. Heat Mass Transf. **57**, 222–230 (2013)

Wagner, E., Stephan, P., Koeppen, O., Auracher, H.: High resolution temperature measurements at moving vapor/liquid and vapor/liquid/solid interfaces during bubble growth in nucleate boiling. In: Proceedings of the 4th International Berlin Workshop on Transport Phenomena with Moving Boundaries, pp. 260–277. VDI Verlag (2007)

Warrier, G.R., Dhir, V.K., Chao, D.F.: Nucleate pool boiling experiment (NPBX) in microgravity: International Space Station. Int. J. Heat Mass Transf. **83**, 781–798 (2015)

Yabuki, T., Nakabeppu, O.: Heat transfer mechanisms in isolated bubble boiling of water observed with MEMS sensor. Int. J. Heat Mass Transf. **76**, 286–297 (2014)

Yabuki, T., Hamaguchi, T., Nakabeppu, O.: Interferometric measurement of the liquid-phase temperature field around an isolated boiling bubble. J. Therm. Sci. Technol. **7**(3), 463–474 (2012)

You, S.M., Simon, T.W., Bar-Cohen, A., Hung, Y.S.: Effects of dissolved gas content on pool boiling of a highly-wetting fluid. ASME J. Heat Transf. **117**, 687–692 (1995)

Zhang, L., Li, Z.D., Li, K., Li, H.X., Zhao, J.F.: Influence of heater thermal capacity on bubble dynamics and heat transfer in nucleate pool boiling. Appl. Therm. Eng. **88**, 118–126 (2015)